The snowflake divertor: a game-changer for magnetic fusion devices?

V. A. Soukhanovskii[1], J.-W. Ahn[2], D. Battaglia[2], R. E. Bell[3], A. Diallo[3], S. Gerhardt[3], R. Kaita[3], S. Kaye[3], E. Kolemen[3], B. P. LeBlanc[3], R. Maingi[2], A. McLean[2], J. E. Menard[3], D. Mueller[3], S. F. Paul[3], M. Podesta[3], R. Raman[4], T. D. Rognlien[1], A. L. Roquemore[3], D. D. Ryutov[1], F. Scotti[3] M. V. Umansky[1]

[1]*Lawrence Livermore National Laboratory, Livermore, CA, USA*
[2]*Oak Ridge National Laboratory, Oak Ridge, TN, USA*
[3]*Princeton Plasma Physics Laboratory, Princeton, NJ, USA*
[4]*University of Washington, Seattle, WA, USA*

Introduction The spherical tokamak (ST) is viewed as a candidate concept for future fusion and nuclear science applications [1, 2]. Divertor experiments in NSTX, a high-power density medium size ST ($R = 0.85$ m; $a = 0.65$ m) with graphite plasma-facing components (PFCs), have demonstrated the features of the inherently compact ST divertor. ITER-scale steady-state peak divertor heat fluxes $q_{pk} \leq 15$ MW/m^2 and $q_{\|} \leq 200$ MW/m^2 have been measured in $I_p = 1.0 - 1.2$ MA discharges heated by 6 MW NBI [3]. As a result of this and other ST- or NSTX-specific geometry features, e.g., a small in/out SOL power ratio, a small divertor PFC area, an open divertor geometry and reduced divertor volumetric (radiated power and momentum) losses, a reduced operating space of the conventional heat flux mitigation techniques, such as the divertor geometry and radiative divertor, has been found [4, 5, 6]. Viewing this as the challenge and the opportunity for plasma-material interface (PMI) development, NSTX research is now focusing on developing the PMI for future devices, in particular for NSTX-Upgrade [7], where steady-state $q_{pk} \leq 25 - 40$ MW/m^2 are predicted based on the present scalings [3].

Experiment and results Recent experimental results obtained with a snowflake divertor (SFD) configuration [8, 9, 10, 11] demonstrate that this novel divertor geometry may not only hold promise for the outstanding pedestal, ELM and PMI issues, but also can be used as a laboratory for pedestal stability and divertor physics studies in existing tokamaks. The SFD magnetic equilibria have been simulated for several tokamaks with existing divertor coils [10]. The number of divertor coils needed for the SFD can be as few as two, an attractive feature for future reactors due to engineering and neutron constraints. In the TCV tokamak, where the SFD has been realized by means of six divertor coils, several advantageous features of the SFD (cf. the standard divertor) have been demonstrated: unchanged L-H power threshold, enhanced stability of the peeling-balooning modes in the pedestal region (and generally an extended second stability region), as well as an H-mode pedestal regime with reduced Type I ELM frequency and slightly increased normalized ELM energy [12, 13, 14, 15]. In initial NSTX experiments, two divertor coils were used to create and maintain the SFD configurations for periods $t \leq 50 - 150$ ms. It was shown that the geometry factors (divertor plasma-wetted surface area, connection length, divertor volume) were significantly increased in the SFD as predicted [8], leading to increased volumetric losses, substantial reductions in divertor heat flux, as well as better impurity screening, and a facilitated access to a radiative divertor detachment [16, 17]. In this paper new magnetic control and divertor results from recent snowflake divertor experiments in NSTX are discussed.

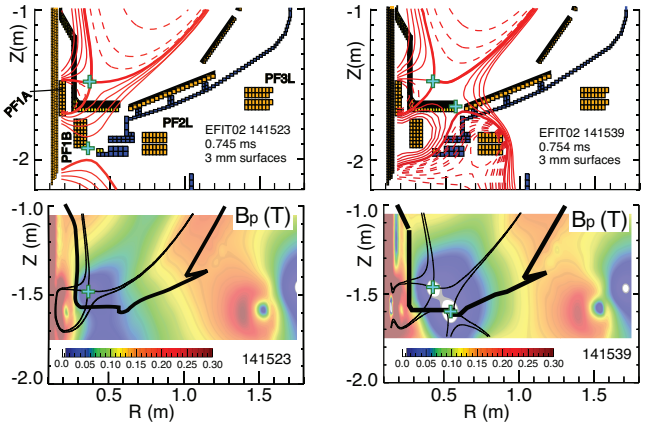

Figure 1: *A comparison of poloidal magnetic flux equilibria and B_p in the standard divertor and the SFD obtained with three divertor coils in NSTX.*

Magnetic control of the SFD configuration is essential in order to maintain the desired orientation and distance between divertor null-points (Fig. 1) in a dynamically changing plasma shape. Analytic advances in the SFD configuration parametrization [18] are being combined with new developments in the NSTX plasma control system [19]: a fast numerical algorithm for finding the null-point positions is being implemented and its testing for real-time SFD control is about to commence. In the meantime, SFD experiments proceeded with divertor magnetic coils operated with pre-programmed currents. SFD configurations with *three* divertor coils (PF1A, PF1B, and PF2L in Fig. 1) were designed using a predictive free-boundary axisymmetric Grad-Shafranov equilibrium solver. The modeling guided the experimental implementation of the three-coil SFD. The steady-state SFD has been obtained for up to 600 ms in highly-shaped 4 MW NBI-heated H-mode plasma discharges of 1.0-1.2 s duration. This enabled a more detailed study of the steady-state SFD properties. Shown in Fig. 1 is a comparison of the high triangularity standard divertor configuration and the SFD obtained from it. The SFD configuration has a larger region with very low B_p: it extends over most of the outer divertor leg as well penetrates deeper into the pedestal region.

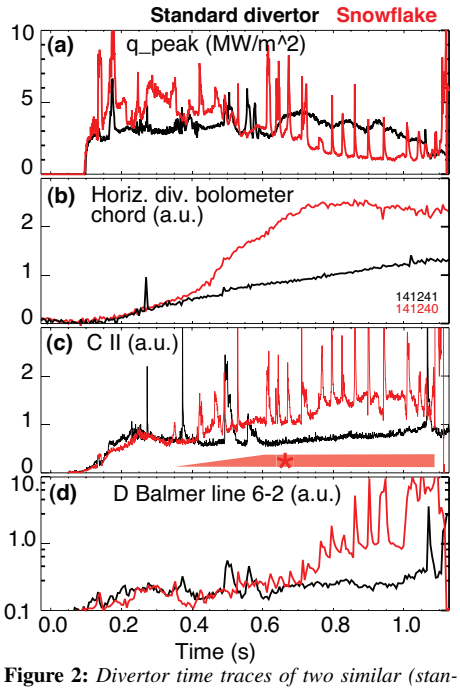

Figure 2: *Divertor time traces of two similar (standard divertor vs. SFD) discharges: (a) peak heat flux; (b) horizontal bolometer signal; (c) C II brightness; (d) Balmer B6 brightness in the strike point region.*

A key issue for future magnetic control of the SFD is keeping the second null-point close to the outer strike point and just below the divertor surface, in order to maintain the magnetic field incidence angle $\gamma \geq 1^\circ$. The angle 1° is considered compatible with the present engineering constraints on the divertor PFC element alignment in order to avoid "hot-spot" formation, melting and/or enhanced physical sputtering at the PFC edges. In the described NSTX experiments, the angle γ in the SFD outer strike point region was $1-2^\circ$, occasionally reaching $\gamma = 0.5-0.9^\circ$.

The SFD formation was always followed by a partial detachment of the outer strike point. Despite the detachment high core confinement was maintained with the three-coil SFD. This was evidenced by the factors $\tau_E \simeq 50-60$ ms, $W_{MHD} \simeq 200-250$ kJ, and the H98(y,2)$\simeq 1$ (estimated using the TRANSP code) similar to those of the standard divertor discharges. Core carbon concentration and radiated power were reduced by up to 30-50 %, apparently as a result of reduced divertor physical and chemical sputtering in the SFD as well as ELMs. During the extended SFD period, medium-to-large size ($\Delta W_{MHD}/W_{MHD} \leq 5-12$ %), Type I, ELMs reappeared, in contrast to the standard divertor discharges where ELMs were suppressed via the use of evaporated solid lithium coatings on divertor PFCs [20].

In the three-coil SFD configurations, a significant reduction of divertor heat flux and increase of carbon radiation were measured. Shown in Fig. 2 are the time traces contrasting divertor measurements in the SFD and in the standard divertor discharges with the SOL power $P_{SOL} = 2.5-3$ MW. In the SFD discharge, the divertor coil currents were increased between 0.350 and 0.550 s, and the SFD was formed at about 0.600-0.650 s. During the SFD formation, the divertor heat flux (shown as the smoothed q_{pk} trace) was decreasing and divertor radiated power P_{rad} (shown as one divertor horizontal bolometer chord signal and the C II brightness) was increasing. If the brightness increase of the Balmer B6 line (measured in the outer strike point region) is taken as an indication of the volumetric recombination onset accompanying the detachment (as in previous radiative divertor experiments [4, 6]), it appears that the partial detachment did not occur until about 650-700 ms. Shown in Fig. 3 are the lower divertor heat flux, C III and CIV brightness profiles at the times of interest in the SFD discharge: in the standard divertor phase

at 0.36 s, during the SFD formation at 0.57 and 0.70 s, and later in the discharge at 0.90 s when the partial detachment was well developed. The peak heat flux was gradually reduced during the SFD formation from 4-7 MW/m^2 to about 2-3 MW/m^2 and further down to 0.5-1 MW/m^2 after the onset of detachment. While after the SFD formation the heat flux profile still showed some peaking in the separatrix region ($R = 0.30 - 0.35$ m) and in the low flux expansion region ($R = 0.55 - 0.65$), it became nearly flat during the detachment suggesting predominantly radiative surface heating. The lower divertor power (obtained by integrating the heat flux profiles) was $P_{div} = 1.8 - 2$ MW before the SFD, $P_{div} = 1.0 - 1.2$ MW during the SFD formation, and $P_{div} = 0.5 - 0.65$ MW later in the radiative phase of the discharge. The C III and C IV brightness profiles showed broadening during the SFD formation; their total brightness was increased by up to 50-100 %. The CII time trace (Fig.2) also showed an additional increase at about 0.70 ms. As carbon radiation is maximized at $T_e \leq 10$ eV, the increase in carbon emission showed that with the SFD formation, divertor plasma became cooler and denser.

In NSTX SFD discharges, the radiative detachment was obtained at or shortly after the SFD formation. The initial NSTX SFD experiments posed a question whether the outer strike point detachment and the associated divertor dissipative loss increase and $q_{||}$ reduction play the key role in the observed significant q_{div} reduction in the SFD. The issue is important for future discharge scenarios involving the SFD, e.g., in the event when the SFD configuration is lost due to plasma motion, or the partial detachment may not be possible due to low SOL collisionality. The partial detachment was previously obtained in NSTX standard divertor discharges using either extrinsic D_2 or CD_4 puffing [4, 6], or in configurations with a low X-point height [5]. Based on the present observations, it appears that the partial detachment, when formed, brings additional dissipative losses; however, the SFD alone (even during the formation phase) reduces steady-state heat flux by 50-60 % and increases divertor P_{rad} by up to 50 %. More experimental and modeling work is needed to understand how the detachment is linked to the SFD effects.

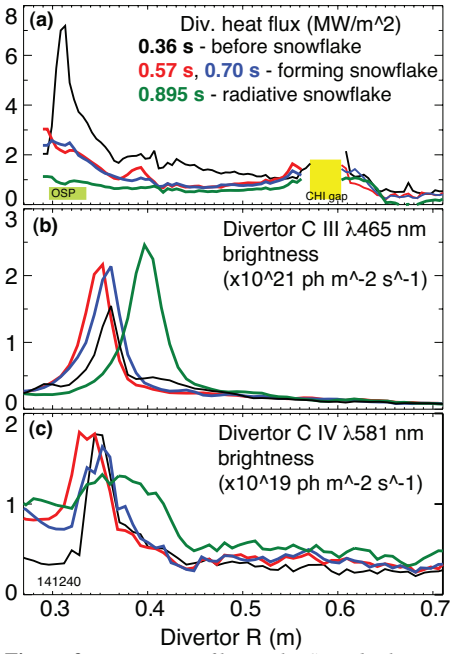

Figure 3: *Divertor profiles in the SFD discharge at 0.36 s, 0.57 s, 0.70 s and 0.895 s: (a) heat flux; (b) C III and (c) C IV brightness.*

Edge transport modeling of the NSTX SFD experiments has commenced using the 2D multi-fluid code UEDGE [21]. The 2D curvilinear meshes spanning $\psi_N = 0.95$-1.04 were generated for the standard divertor and for the snowflake-minus configurations described in detail in Ref. [16, 17] as shown in Fig. 4. A core-plasma interface was assumed having $T_e = 120$ eV, $T_i = 120$ eV, and $n_e = 4.5 \times 10^{19}$ m^{-3}. Classical SOL parallel transport and anomalous radial transport with $\chi_{e,i} = 0.5$ m^2/s and $D = 0.25$ m^2/s were assumed for the energy and ions. A carbon concentration of 3 % and the PFC recycling coefficient of 0.95 were used. Shown in Fig. 4 is a comparison of modeled divertor profiles. The simulations indicated a tendency for colder, denser plasma in the SFD vs. the standard divertor; however, more work is needed to match the experimental profiles and use the model in the interpretive sense. While the shown profiles did not indicate the partial detachment observed in the experiment, large reductions in T_e and T_i, particle and heat fluxes were seen in the high flux expansion zone of the SFD. An edge transport modeling study of the SFD and the standard divertor in the DIII-D geometry [11, 22] concluded that 1) the heat flux in the SFD divertor was reduced stronger than just the ratio of the plasma-wetted areas; it also included the reduction due to increased volumetric losses; 2) the detachment threshold expressed in terms of the edge n_e was lower in the SFD. Both of these modeling results are qualitatively consistent with the NSTX experiment.

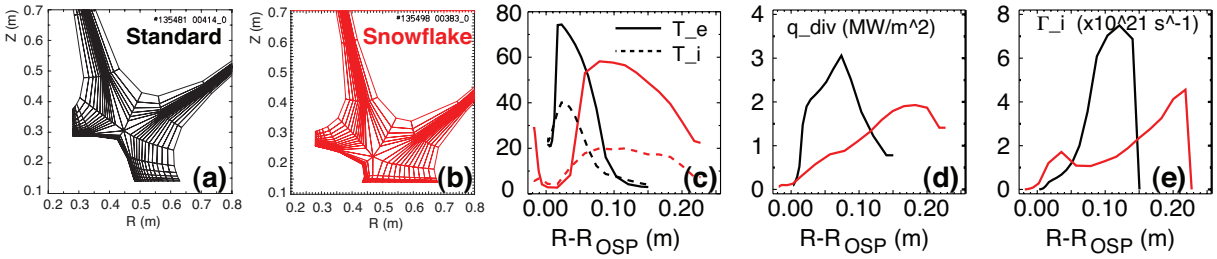

Figure 4: UEDGE model results of the standard divertor (black lines) and SFD (red lines): (a, b) divertor region computation mesh; divertor plate profiles: (c) T_e, T_i, (d) heat flux density; (e) particle flux density.

Summary Recent results from NSTX indicate that the snowflake divertor may be a viable solution for the outstanding tokamak PMI issues. The SFD appears to be compatible with high-confinement core plasma operation, while being very effective in divertor heat flux mitigation and impurity screening. Research in NSTX is now focusing on details of the heat transport and power balance in the SFD, the SFD operation with active pumping [23], the pedestal stability and ELMs, and the magnetic control of the SFD. Plasma discharge scenarios having lower and upper SFD are being developed to address the needs of future ST-based devices.

Acknowledgments We thank the entire NSTX Team for the technical, engineering and computer support as well as the plasma, NBI and diagnostic operations. This work was performed under the auspices of the U.S. Department of Energy under Contracts DE-AC52-07NA27344, DE AC02-09CH11466, DE-AC05-00OR22725, DE-FG02-08ER54989.

References

[1] PENG, Y.-K. et al., Plasma Phys. Control. Fusion **47** (2005) 263.
[2] GOLDSTON, R. et al., in *Fusion Energy 2008 (Proc. 22nd Int. Conf. Geneva, 2008)*, CD-ROM file FT/P3-12, Vienna:IAEA.
[3] GRAY, T. K. et al., J. Nucl. Mater., at press (2011).
[4] SOUKHANOVSKII, V. et al., Phys. Plasmas **16** (2009) 022501.
[5] SOUKHANOVSKII, V. A. et al., High flux expansion divertor studies in NSTX, in *36th EPS Conf. on Plasma Phys., Sofia, Bulgaria*, 2009, http://arxiv.org/abs/0912.4281.
[6] SOUKHANOVSKII, V. et al., Nucl. Fusion **49** (2009) 095025.
[7] MENARD, J. E. et al., Physics design of the NSTX upgrade, in *Proc. 37th EPS Conf. on Plasma Phys.*, Europhys. Conf. Abstr., Vol. 34A, Paper P2.106, Belfast, Ireland, 2010.
[8] RYUTOV, D., Phys. Plasmas **14** (2007) 064502.
[9] RYUTOV, D. et al., Phys. Plasmas **15** (2008) 092501.
[10] RYUTOV, D. et al., in *Fusion Energy 2008 (Proc. 22nd Int. Conf. Geneva, 2008)*, CD-ROM file IC/P4-8, Vienna:IAEA.
[11] UMANSKY, M. et al., Nucl. Fusion **49** (2009) 075005.
[12] PIRAS, F. et al., Plasma Phys. Control. Fusion **51** (2009) 055009.
[13] PIRAS, F. et al., Plasma Phys. Control. Fusion **52** (2010) 124010.
[14] PIRAS, F. et al., Phys. Rev. Lett. **105** (2010/10/08) 155003.
[15] MEDVEDEV, S. et al., Contrib. Plasma Phys. **50** (2010) 324.
[16] SOUKHANOVSKII, V. A. et al., J. Nucl. Mater., at press (2011).
[17] SOUKHANOVSKII, V. et al., Nucl. Fusion **51** (2011) 012001.
[18] RYUTOV, D. et al., Plasma Phys. Control. Fusion **52** (2010) 105001.
[19] KOLEMEN, E. et al., in *Fusion Energy 2010 (Proc. 23nd Int. Conf. Daejon, 2010)*, CD-ROM file EXD/P3-18, Vienna:IAEA.
[20] MAINGI, R. et al., Phys. Rev. Lett. **103** (2009) 075001.
[21] ROGNLIEN, T. D. et al., J. Nucl. Mater. **196-198** (1992) 347.
[22] UMANSKY, M. et al., Contrib. Plasma Phys. **50** (2010) 350.
[23] SOUKHANOVSKII, V. A. et al., in *Fusion Energy 2010 (Proc. 23nd Int. Conf. Daejon, 2010)*, CD-ROM file EXD/P3-32, Vienna:IAEA.